Article

Journal of Vibration and Control
2022, Vol. 28(19-20) 2607–2624

DOI: 10.1177/10775463211017721
journals.sagepub.com/home/jvc
SAGE

Robust multi-steps input command for liquid sloshing control

Abdullah Alshaya and Adel Alshayji

Abstract

A robust input command based on multiple steps for eliminating the residual vibrations of a multimode linear system is proposed. Only the system resonant frequencies are needed to determine the step magnitudes in the shaped command. The command duration is selectable to help in designing an optimum command that compensates between the reduction in the transient vibration, the enhancement in the command robustness, and the increase in the total maneuver time. The induced transient and residual sloshing oscillations of a suspended water-filled container are suppressed using the proposed command. The dynamics of the sloshing is numerically simulated using finite element method that accommodates the interactions between the fluid, structural, and multi-body dynamics. A short move time penalty is incurred with the price of significant reduction in the liquid sloshing. The performance of the shaped command to the system parameters and the robustness to their uncertainty are investigated. An improved robust input command in the presence of uncertainties in the cable length and water depth is also introduced. The effectiveness and excellence of the proposed command is demonstrated through a comparison with multimode zero-vibration input shaper and time-optimal flexible-body control.

Keywords

Sloshing, fluid–structure interaction, finite-element analysis, liquid suppression, vibration control, command shaping, open-loop control, overhead crane

1. Introduction

The problem of sloshing induced by transferring liquid container in automated systems, for example, transferring of a molten metal, attracts the attentions of many researchers. The rapid movement, as in rest-to-rest maneuver, of a liquid-filled container is a challenging control problem because the induced sloshing may compromise safety, degrade the positioning accuracy, result in economic loss, and slow the operational process. Liquid-filled containers are usually conveyed in a relatively slow motion and without using the full input capability to limit the induced transient sloshing. Although there are several passive methods to limit sloshing such as using baffles and/or dividing a large container into a number of smaller ones, these techniques add complexity into the problem and do not completely eliminate the sloshing effects (J.R. Cho and Lee, 2004; Hasheminejad et al., 2014; Wang et al., 2016). Therefore, it is desirable to use active controlling techniques to allow higher speeds and make the operations more efficient and accurate by reducing the transient fluid oscillations (reduce the operational risks when transferring hazardous liquids) and diminishing the residual sloshing (reduce the wasting time before safely issuing the next command and hence reduce the overall operational time). One of the appealing control approaches to tackle this class of problems with fast maneuvering and accurate positioning is the open-loop feedforward techniques.

Unlike closed-loop feedback techniques which necessitate the need of using sensors to record the real-time measurements of the system's states, the open-loop control techniques are extensively used to reduce the induced transient and residual vibrations of the controlled system. Command shaping, an open-loop control technique, is based on designing the system input by specifying the desired output trajectory of a vibratory system (Alhazza and Masoud, 2016; Masoud and Alhazza, 2017). Input shaping, the most commonly used command shaping technique, involves convolving a sequence of timed impulses designed

Mechanical Engineering Department, College of Engineering and Petroleum, Kuwait University, Kuwait

Received: 23 September 2020; accepted: 24 April 2021

Corresponding author:
Abdullah Alshaya, Department of Mechanical Engineering, College of Engineering and Petroleum, Kuwait University, Alkhaldeya Campus, P.O. Box 5969, Safat 13060, Kuwait.
Email: abdullah.alshaye@ku.edu.kw

from the knowledge of the system's dynamics with system's general input command to mitigate the excited vibrations in a single (N. C. Singer and W. P. Seering, 1992; Singer and Seering, 1990; Singhose and Pao, 1997) and multimode systems (Hyde, 1990; Mohamed and Tokhi, 2003; Singh and Vadali, 1995). The most drawbacks of these techniques are their robustness to uncertainties in the system parameters and the increase in the move time (Vaughan et al., 2008).

Sloshing in a laterally moving and suspended water-filled containers was suppressed using several controlling methods: H^{∞} control theory (K. Yano and K. Terashima, 2001), notch filter (A. Kaneshige et al., 2009), command shaping (Alshaya and Alghanim, 2020; Alshaya and Almujarrab, 2020), and input shaping (AlSaibie and Singhose 2013; Murthy et al., 2012; Pridgen et al., 2013). The input shapers were convolved with a smooth command to suppress multiple sloshing modes (Baozeng and Lemei, 2014; Xing and Huang, 2020; Zang et al., 2015). These convolved commands were also applied to a three-dimensional linear and nonlinear sloshing dynamics models (Huang and Zhao, 2018; Zang and Huang, 2015). Biagiotti et al. (2018) used a harmonic smoother composed of input shaper and low-pass filter to shape the input trajectory in the runtime process. Most of the controlling techniques were designed based on the equivalent mechanical models: pendulum damper models (Baozeng and Lemei, 2014; Biagiotti et al., 2018; Kaneshige et al., 2009; Yano and Terashima, 2001) or mass–spring–damper systems (AlSaibie and Singhose, 2013; Alshaya and Alghanim, 2020; Alshaya and Almujarrab, 2020; Murthy et al., 2012; Pridgen et al., 2013; Reyhanoglu and Rubio Hervas, 2013). These models are based on the assumption that the liquid behaves in its fundamental mode predominantly. Alternatively, Aboel-Hassan et al. (2009) used finite element method (FEM) proposed by Arafa (2007) to model the fluid–structure interaction and used command shaping to suppress the induced sloshing. Several numerical methods, such as finite differences and smoothed particle method, could also be applied to model the fluid–structure interaction and predict the sloshing dynamics (J.R. Cho and Lee, 2004; Hasheminejad et al., 2010; Brar and Singh, 2014).

Most of the existing literature are focused on one or more of the following aspects: minimizing the transient elevation of the free surface level, reducing the maneuver time, minimizing the residual sloshing, reducing the settling time, and/or enhancing the robustness of the controlled input command. The aim of this study is to improve the suppression of the induced sloshing of a moving suspended water-filled container in several aspects. First, an equidistant multistep input command (MSIC) for eliminating the residual vibrations of a multimode linear system is proposed. The amplitudes of the generated steps are only functions of the system natural frequencies where the command length can be adjusted to provide such optimal command that compensates between the vibration-reduction, the command robustness, and the total move time. Second, the liquid sloshing is modeled using FEM to numerically predict the elevation of the free-surface liquid level and account for the nonlinearities embedded in the model rather than using a linear assumption such as in the equivalent mechanical models. The corresponding resonant frequencies up to three sloshing frequencies are determined based on the fast Fourier transform (FFT) and were used to design the shaped commands. Third, the proposed command performance is improved by enhancing its robustness to the uncertainties in the system parameters, and its efficacy is demonstrated by a comparison with multimode zero-vibration (MMZV) input shaper and time-optimal flexible-body control.

2. Theoretical development

The problem of suppressing the induced sloshing in a suspended rigid-walled container with a width W and height H and conveyed by an overhead crane, that is, modeled as a slider jib and governed with a predefined acceleration command, $\ddot{u}(t)$ is considered, Figure 1. The container is filled with a water of depth h measured from the bottom of the container to the undistributed free surface, $y = 0$. A rigid link of length l connects the container with the horizontally moving slider. The motion of the jib makes the container to swing in the xy-plane with an oscillation angle $\theta(t)$ and the free surface of the inside water to oscillate with lateral displacement $\eta(x, t)$ because of the water sloshing.

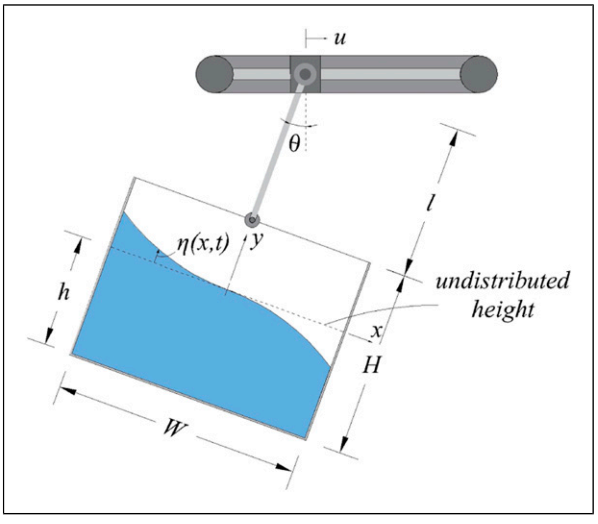

Figure 1. Liquid sloshing in a conveyed rigid-walled water-filled container by an overhead crane.

2.1. Multi-steps input command

The sloshing dynamics without considering the heaving and pitching excitations can be modeled as a multimode linear system (Ibrahim, 2005). These assumptions are valid if the oscillation angle of the pendulum system is small. The corresponding governing equations of motion where the system input is the jib acceleration, $\ddot{u}(t)$, can be written in terms of the time-dependent generalized principal (decoupled) coordinate vector, $\mathbf{q}(t) = \{ q_1(t) \quad q_2(t) \quad \cdots \quad q_N(t) \}^T$, as

$$\ddot{q}_i(t) + \omega_i^2 q_i(t) = p_i \ddot{u}(t), \quad \text{for} \quad i = 1, 2, \ldots, N \tag{1}$$

where ω_i is the system natural frequency and p_i is a constant. The first step toward generating a system input which eliminates the residual vibration of a multimode system is to specify the system response to a multi-steps input command (MSIC) with m steps. The MSIC can be written in general as

$$\ddot{u}(t) = \sum_{k=1}^{m} (A_k - A_{k-1}) H_{\tau_k}, \quad A_0 = 0 \tag{2}$$

where A_k is the step amplitude in the interval $[\tau_k, \tau_{k+1}]$ and $H_{\tau_k} = H(t - \tau_k)$ is the Heaviside function. For convenience, the command is assumed to start at $t = 0$, and hence, $\tau_1 = 0$. Substitution of equation (2) into (1) and solving the resultant differential equations using Duhamel integral with zero initial conditions yield the following general responses, and their corresponding time derivatives, namely

$$q_i(t) = \frac{p_i}{\omega_i^2} \sum_{k=1}^{m} (A_k - A_{k-1}) [1 - \cos(\omega_i (t - \tau_k))] H_{\tau_k} \tag{3}$$

$$\dot{q}_i(t) = \frac{p_i}{\omega_i} \sum_{k=1}^{m} (A_k - A_{k-1}) \sin(\omega_i (t - \tau_k)) H_{\tau_k} \tag{4}$$

for $i = 1, 2, \ldots, N$.

2.2. Command designing

The point-to-point maneuvers in modern industrial automation systems are used in automated lines and repeated cycles. These cycles consist of an acceleration stage where the jib accelerates from rest to a cruising velocity, v_f, a cruising stage where the jib moves with a constant velocity, and finally a deceleration stage where the jib decelerates from the cruising velocity to final rest position. The classical multimode zero-vibration input shapers (MMZV) necessitates the need of either convolve many single input shapers or solve, simultaneously, a system of nonlinear equations for the impulse magnitudes and their corresponding times (Hyde, 1990). Furthermore, the time-optimal flexible-body control (TOZV) which uses the full actuator capability with rapid switching times also necessitates the need of numerical optimization to determine these switching times (Singer and Seering 1992). Unlike MMZV and TOZV, the proposed command is assumed to have equidistant steps where in this case the amplitudes are unknown and can be determined from solving a system of simultaneous linear equations.

To enforce the jib accelerating from the rest to the cruising velocity, the integration of the MSIC, equation (2), from $t = 0$ to the end of the acceleration stage, $t = \tau_a$, should be equal to v_f, that is

$$\int_0^{\tau_a} \ddot{u}(t)\, dt = \sum_{k=1}^{m} A_k \Delta\tau = v_f \tag{5}$$

where $\Delta\tau = \tau_k - \tau_{k-1}$ is the time length for each of the m equidistant steps and $\tau_a = m\Delta\tau$ is the command time length. The principal coordinates, q_i and $\dot{q}_i$, at the end of the acceleration stage have to be set to zero to eliminate the residual vibrations from the all N excited modes of the system in equation (1). This necessitates the need of using $m = 2N + 1$ steps in equation (2). Substituting $t = \tau_a$ into equations (3) and (4) and imposing the condition of equation (5) form a system of simultaneous linear equations

$$\mathbf{M}\mathbf{c} = \mathbf{b} \tag{6}$$

where $\mathbf{c} = \{ A_1 \quad A_2 - A_1 \quad \cdots \quad A_{2N+1} - A_{2N} \}^T$ and $\mathbf{b} = \{ 0 \quad \cdots \quad 0 \quad v_f/\Delta\tau \}^T$ are column vectors, and matrix $\mathbf{M}$ is defined as

$$\mathbf{M}(2i - 1, k) = 1 - \cos(\omega_i(\tau_a - (k - 1)\Delta\tau)) \tag{7a}$$

$$\mathbf{M}(2i, k) = \sin(\omega_i(\tau_a - (k - 1)\Delta\tau)) \tag{7b}$$

$$\mathbf{M}(2N + 1, k) = 2N + 2 - k \tag{7c}$$

where $i = 1, 2, \ldots, N$ and $k = 1, 2, \ldots, 2N + 1$.

Designing MSIC necessitates the need of solving for the coefficient vector $\mathbf{c}$ from equation (6) once the coefficient matrix $\mathbf{M}$ and the column vector $\mathbf{b}$ are known. The latter, equation (7), are only functions of the system natural frequencies, and the command time length, τ_a, is independent from the system natural frequencies. Even though that decreasing the command length will consequently make the response faster, it will increase the system sensitivity and affect the overall performance. An optimum command is achieved, that is, minimum maneuver time, T, by using the full capability of the input command. Therefore, the time length should be selected such that all the amplitudes of the MSIC are within the maximum acceleration of the driven motor, that is, $|A_k| \le a_{\max}$ for all values of k.

Once the amplitudes of the MSIC are evaluated from equation (6) while ensuring that $|A_k| \le a_{\max}$, the distance that the jib moves during the acceleration stage, s_a, is

$$s_a = \int_0^{\tau_a} \int_0^{\hat{t}} \ddot{u}(t)\, dt\, d\hat{t} = \frac{1}{2} \sum_{k=1}^{m} (\tau_a - k\Delta\tau)^2 (A_k - A_{k-1}) \tag{8}$$

The deceleration profile of the jib is the inverted version of the acceleration profile, that is, $\ddot{u}_d(t) = -\ddot{u}_a(t)$, hence $s_d = s_a$ and $\tau_d = \tau_a$. To ensure that the jib travels a distance, d, it should cruise a distance $s_c = d - 2s_a$ with a time duration $\tau_c = s_c/v_f$. Therefore, the total move time is $T = 2\tau_a + \tau_c$. If the traveled distance, d, is short or the command length, τ_a, is slow, the shaped command may not use the driven motor maximum capabilities (velocity and/or acceleration). It is worth to mention that the proposed MSIC is not only restricted to suppressing sloshing in a suspended container and it can be applied to other multimode linear systems.

3. Finite element model

The water sloshing in a rigid-walled container that is conveyed by an overhead crane as shown in Figure 2(a) was numerically simulated using COMSOL Multiphysics® software COMSOL (2019). The densities and dynamic viscosities of the water and air are 998.2 and 1.2043 kg/m^3, and 1.009×10^{-3} and 1.814×10^{-5} Pa·s, respectively. Steel structure with a density of 7850 kg/m^3 was used to model the tank frame and the rigid link.

The multi-body dynamics and solid mechanics modules were used to model the overall structure with a hinge located at point A as shown in Figure 2(a). The container, and the fluid inside, was moved by an input horizontal acceleration applied at the point A. The flow motion of the incompressible fluids, water and air, was modeled using laminar single phase flow module that solves the 2D Navier–Stokes equations. A negative vertical acceleration was applied to simulate the gravitational effect. Both fluids were assumed initially to be stationary, with zero velocity and atmospheric pressure. No-slip boundary conditions were applied at the internal walls where the interaction between the fluid and the inner side of structures occurs. The interaction between the water and air movements was modeled using the two-phase flow level set. This model is based on assuming that no flow is allowed to cross the container internal walls. The interactions between the multi-body dynamics and laminar flow were coupled by the means of fluid–structure interaction. The induced surface tension forces between the water and air because of the free-surface flow were applied into the momentum equations in the laminar flow model.

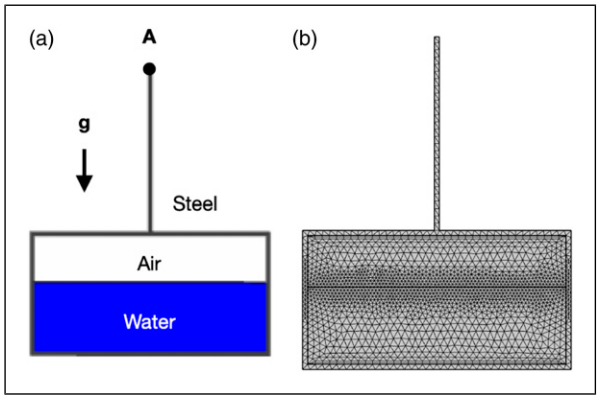

Figure 2. (a) Materials used in the rigid-walled water-filled container and the (b) mesh used in computational domain; 14 vortex elements, 434 boundary elements, and 3326 domain elements.

Simple triangular elements were used to mesh the structural part, where a mix of triangular and rectangular elements was used to mesh the fluid parts. The rectangular elements were used to solve for the boundary layer formed between the fluid and structure. The mesh consists of 14 vortex elements, 434 boundary elements, and 3326 domain elements with a special concentration on the interface between the water and air as shown in Figure 2(b). Elements located at the interface were used to track the water and air interactions and capture the water sloshing when the free-surface level changes. To accommodate the motion of the container structure and the motion of the fluid flow inside the container, a moving and deformable mesh was used.

Two solver steps, phase initialization and time-dependent steps, were used to solve the constructed fluid–structure model. The first step is based on using two-phase flow level set model and the moving mesh to initialize each material in its corresponding location inside the computational domain, Figure 2(a). This step is performed for every time the water level changes. The second step involves solving all the modules in the model simultaneously to provide the time-dependent solutions. The solver used parallel sparse direct solver to solve for linear systems in flow velocity, pressure field, level set variable of the two phase flow, and special mesh displacement. This solver is robust and is usually used for highly dependent variables. For the structure displacement field, multifrontal massively parallel sparse direct solver was used. All above mentioned variables were solved in segregated manner, which made possible to split the solution process into substeps. Each step uses a damped version of Newton's method. In such a highly nonlinear problems, especially for multiphase flow, the time stepping solver uses the backward differentiation formula with nonlinear controller for more efficient time-step control. The model was validated by comparing the predicted resonant frequencies when the container is laterally excited with sloshing frequencies formula proposed by Graham and Rodriguez (1952).

4. Numerical results

The MSIC can be generated using only the values of the natural frequencies of the suspended water-filled container

without the need of a complete model. The natural frequencies of the suspended system are functions of (but not limited to) liquid depth, cable length, liquid type, and container dimensions and geometry. For the current numerical experiment, a rectangular-shaped container which is filled with water and has dimensions listed in Table 1 is considered, Figure 1. The maximum acceleration, maximum velocity, and the total traveled distance of the jib are $a_{\max} = 1.0$ m/s^2, $v_f = 0.4$ m/s, and $d = 1.5$ m, respectively. The free-surface water level at the right edge point $\eta(W/2, t)$ is considered to be the critical location at which the water level should be reduced. The water damping effect is neglected such that the present case can be considered as the worst-case scenario. For instance, one can consider the water damping by finding each modal damping coefficient from the frequency response function using the quality factor approach. To ascertain the effects of water depth, h, and cable length, l, in the controlling design, different ratios of h/W and l/H are considered. Furthermore, the sensitivity of the shaped MSIC to the changes in water depth and cable length is also investigated. The response of the suspended water-filled container to the shaped MSIC is obtained from the FEM.

4.1. Response of time-optimal of rigid-body motion

The time-optimal of rigid-body motion (TORB) command, considered as the unshaped (uncontrolled) command, represents the fastest possible command profile which is based on using the full input acceleration and velocity capabilities of the actuator regardless of the output response (see Figure 5(c) and (d)). The corresponding total maneuver time is $T = 4.15$ s. For the suspended system which is started from rest and subjected to TORB command, the responses of the swing angle, $\theta(t)$, and the free-surface water level, $\eta(W/2, t)$, from FEM are illustrated in Figure 3 using different water depth ratios. Even though the jib was stopped at $t = 4.15$ s, the container was still swinging and the inside water was still sloshing (the shaded area in Figure 3). The increasing of the water depth ratios, that is, increasing the mass of the inside water, reduces the transient and residual sloshing of the free-surface water level. However, no significant effect is noticed on the response of the swing angle with the increase in the water depth ratios. It is worth noting that the maximum swing angle of the TORB is within the acceptable range of the linearity assumption (less than 10°).

Table 1. Dimensions of the container and the attached rigid link.

Container	Value	Link	Value
Width, W (cm)	25	Width (cm)	0.5
Height, H (cm)	12.5	Length, l (cm)	37.5
Thickness (cm)	0.5	Thickness (cm)	0.5
Depth (cm)	25	Depth (cm)	25

4.2. Shaped multi-steps input command

The MSIC is designed to convey the suspended water-filled container shown in Figure 1 from its rest position, that is, zero initial conditions, to a final position while inducing minimal transient and residual oscillation. Resonant frequencies are determined by giving the system an arbitrarily initial disturbance and obtaining the FE-predicted time history of the free-surface water elevation at the edge of the container, $\eta(W/2, t)$. Using a FFT with a time step of 0.01 s, the amplitude spectrum of the water level for the depth ratios of 0.1 and 0.3 is illustrated in Figure 4. Based on the FE-determined resonant frequencies of the suspended system, the corresponding amplitudes of the MSIC can be determined from equation (6) and independent of the command duration. The following subsections demonstrate the capability of the MSIC to reduce the residual and

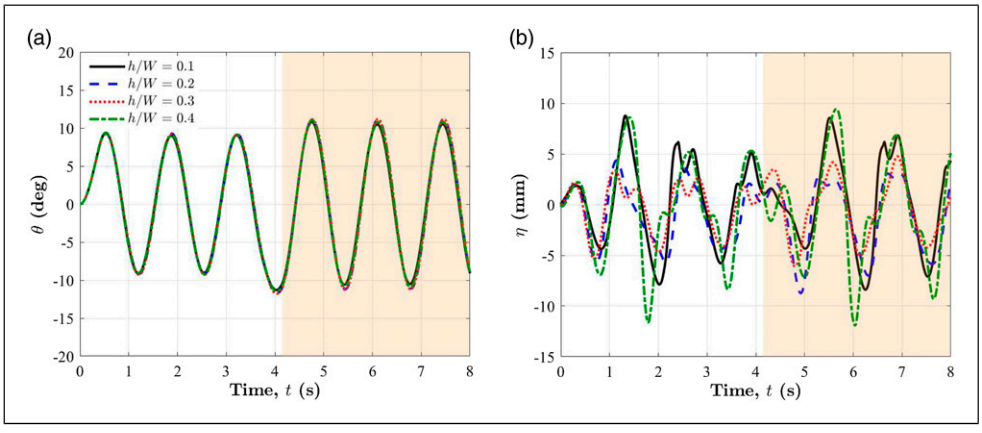

Figure 3. Swing angle and free-surface water elevation for time-optimal of rigid-body motion command using different depth ratios h/W ($l/H = 3$). (a) Swing angle. (b) Free-surface water level.

transient sloshing with different command lengths, water depths, number of used resonant frequencies, and cable lengths.

4.2.1. Variation of command lengths. The MSIC is designed using different depth ratios, h/W, and command lengths, τ_a. For a water depth ratio of $h/W = 0.1$, the MSIC was generated based on the three resonant frequencies in Figure 4(a); $\omega_1 = 4.707$ rad/s, $\omega_2 = 6.275$ rad/s, and $\omega_3 = 10.98$ rad/s. Therefore, $m = 7$ steps are needed in MSIC, equation (2), to eliminate the corresponding residual oscillation of the three considered modes while ensuring the jib reaches its maximum velocity, v_f, at the end of the acceleration command. The smallest command length such that all the amplitudes are within the predefined maximum acceleration, $a_{\max}$, is $\tau_a = 1.39$ s. Figure 5 shows the generated MSIC profile and

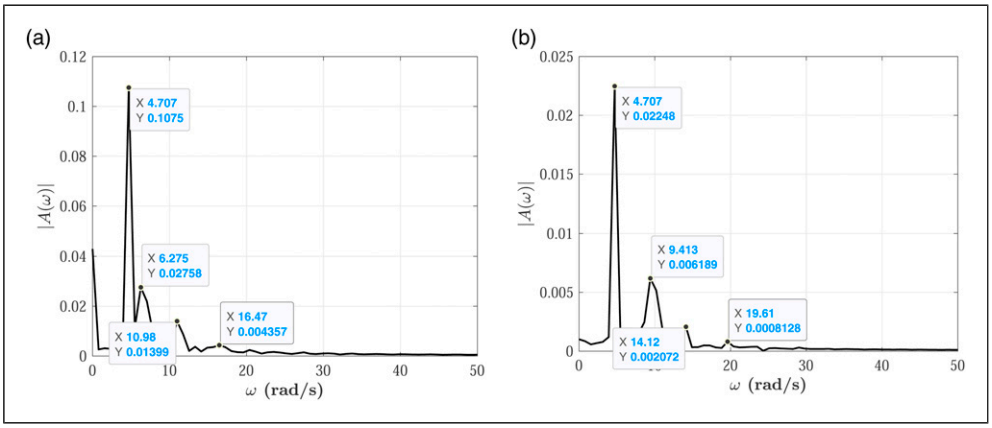

Figure 4. Amplitude spectrum of the free-surface water level, $\eta(W/2, t)$, using fast Fourier transform for different water depth ratios ($l/H = 3$). (a) $h/W = 0.1$. (b) $h/W = 0.3$.

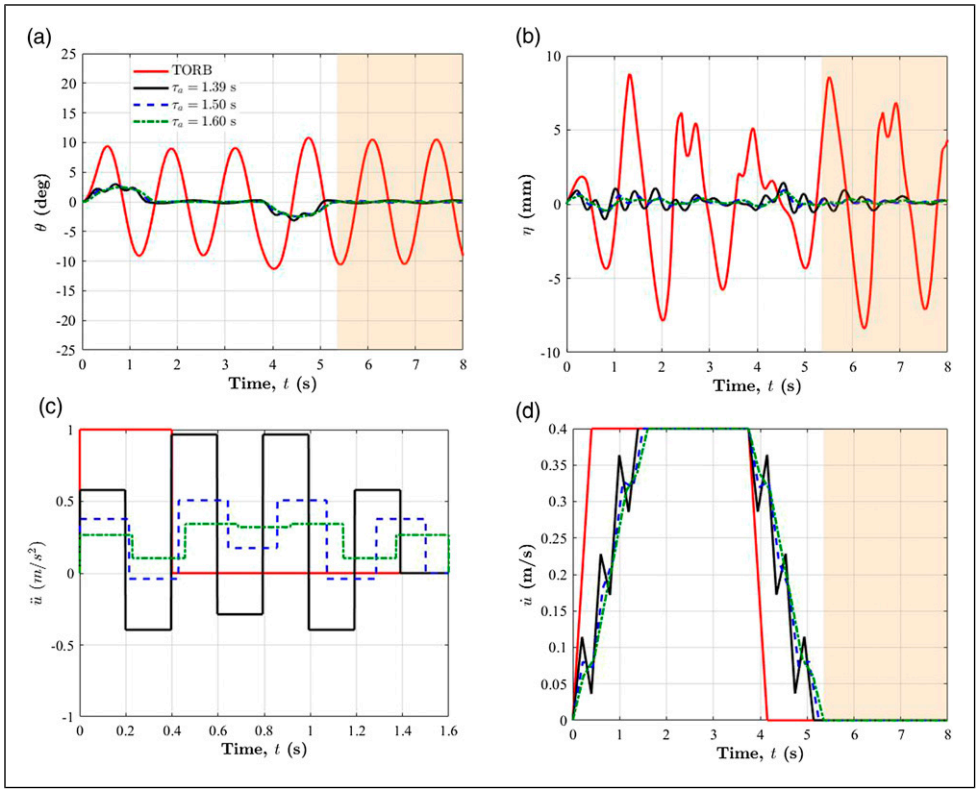

Figure 5. Multi-steps input command profiles and their corresponding dynamics responses using different command lengths ($h/W = 0.1$ and $l/H = 3$). (a) Swing angle. (b) Free-surface water level. (c) Jib acceleration. (d) Jib velocity.

the corresponding dynamics responses using the smallest command length (1.39 s) and two additional command lengths, 1.50 and 1.60 s. For all subsequent figures, the shaded areas represent the transient response of the slowest command, for example, τ_a = 1.60 s in Figure 5. Furthermore, only the input profile in the acceleration stage is illustrated. It is clear from Figure 5(a) that the swing angle is almost eliminated in the cruising and residual stages. As a result, the water level is significantly reduced comparing to the TORB response in these two stages, Figure 5(b).

Figure 6 shows the generated MSICs and their corresponding dynamics responses with $h/W = 0.3$. Based on the four resonant frequencies in Figure 4(b), nine amplitudes in the MSIC were generated. The smallest command length is 1.14 s that within none of the generated amplitudes exceeded the predefined maximum acceleration value. Even though that the residuals of the swing angle and water level are not completely eliminated at the end of the command stages, the residuals of higher command lengths (1.20 and 1.30 s) are almost diminished, Figure 6(a) and (b).

The amount of the induced vibration *during* the move rather than at the end of a maneuver is an important quantity to measure. Decreasing sloshing during the move can increase the life time of the container and improve the trajectory following of the endpoint. The FEM generates the response of the water level at the edge of the container using n = 801 data points (Δt = 0.01 s). The root-mean-square (rms) of the FE-predicted water level response, η_{rms}, is used as a quantitative measurement of the water level oscillation. The corresponding rms values of the water level for TORB command using $h/W = 0.1$, 0.2, 0.3, and 0.4, Figure 3, and l/H = 3 are 4.2886, 3.4095, 2.7341, and 4.9713 mm, respectively. The maneuver time for the fastest possible shaped MSIC with a water depth ratio of $h/W = 0.1$ is T = 5.14 s (corresponding to τ_a = 1.39 s) which is 23.9% slower than the TORB command (T = 4.15 s). However, a reduction of 89.9% in the water level oscillation was achieved (0.4479 vs 4.2886 mm). Increasing the command lengths, that is, making the response slower, significantly reduces the water level oscillation, Table 2. With the increasing in water depth, the shaped MSIC becomes faster and the reduction in the water oscillations becomes smaller, Table 2.

4.2.2. Variation of water depth. The responses of the swing angle and water level using the fastest shaped MSIC profiles generated from different water depth ratios are shown in

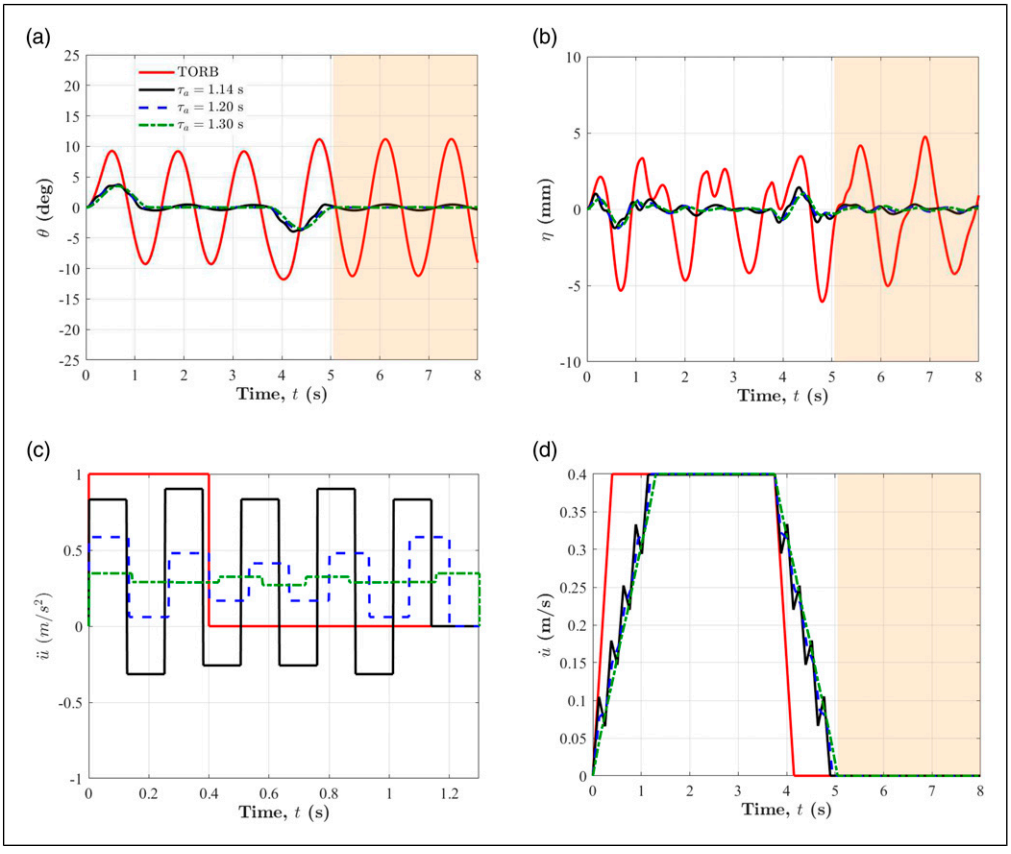

Figure 6. Multi-steps input command profiles and their corresponding dynamics responses using different command lengths (h/W = 0.3 and l/H = 3). (a) Swing angle. (b) Free-surface water level. (c) Jib acceleration. (d) Jib velocity.

Figure 7. The absolute residuals of the swing angle in the cruising stage and at the end of the command are less than one degree, Figure 7(a). Similarly, the residuals of the water levels are less than 1 mm and the maximum transient oscillation did not exceed 1.5 mm, Figure 7(b). The shaped MSICs used to produce the dynamics responses use the full capabilities of the jib driven motor.

4.2.3. Higher sloshing models. The fundamental frequency of the suspended system with dimensions listed in Table 1 corresponds to the swing motion where the higher frequencies correspond to the sloshing modes. Using many resonant frequencies when designing the input command could increase the reduction in the water oscillation but with the cost of the increase in the maneuver time. Figure 8 shows the response of MSICs designed based on two (5 steps; τ_a = 1.32 s), three (7 steps; τ_a = 1.39 s), and four (9 steps; τ_a = 1.37 s) modeled resonant frequencies which are depicted in Figure 4(a). Their corresponding maneuver times are 5.07, 5.14, and 5.13 s, and their rms wave oscillations are 0.3986, 0.4464, and 0.3792 mm for $h/W = 0.1$. The oscillation of the water level was reduced from 0.3986 to 0.3792 mm (4.87%) with the price of increasing in the maneuver time from 5.07 to 5.13 s (1.18%). For a water depth ratio of 0.3 (results are not shown here), the wave oscillation was reduced 34.9% with 2.31% increase in the maneuver time when using four resonant frequencies rather than two frequencies. Even though considering only the frequency corresponding to the swing motion and fundamental sloshing frequency in the command-designing has a major impact in reducing the residual oscillations, using the higher sloshing modes offers significant reduction in the residual and transient oscillations.

Table 2. Command lengths, maneuver times, and root-mean-square values of the free-surface water oscillations for different depth ratios (T_{TORB} = 4.15 s).

		Maneuver time		Water level	
h/W	τ_a (s)	T (s)	Increase (%)	η_{rms} (mm)	Reduction (%)
0.1	1.39	5.14	23.9	0.4479	89.6
	1.50	5.25	26.5	0.2910	93.2
	1.60	5.35	29.0	0.2537	94.1
0.2	1.17	4.92	18.6	0.4609	86.5
	1.30	5.05	21.7	0.3392	90.1
	1.40	5.15	24.1	0.2898	91.5
0.3	1.14	4.89	17.9	0.4025	85.3
	1.20	4.95	19.3	0.3644	86.7
	1.30	5.05	21.7	0.3221	88.2
0.4	1.77	5.12	32.9	0.2879	94.2
	1.90	5.65	36.1	0.2387	95.2
	2.00	5.75	38.6	0.2499	95.0

4.2.4. Variation of cable length. Figure 9 shows the dynamics responses with depth ratio of $h/W = 0.1$ and different cable length ratios, l/H. The corresponding rms values of the water level for TORB command using l/H = 1, 2, 3, and 4 and h/W = 0.1 are 3.003, 5.576, 4.2886, and 5.380 mm, respectively. For l/H = 1, the smallest command length is τ_a = 0.89 s, and the corresponding maneuver time and the rms of the free-surface water levels are 4.64 s and 0.2500 mm, respectively, Table 3. The shaped MSIC reduces the water sloshing, that is, the rms of the transient and residual water levels, from 3.003 to 0.2500 mm (91.7% reduction) with the price of 11.8% (4.15 vs 4.64 s) increase in the operational time, Figure 9(b). Consequently, the maximum swing angle of the controlled response is 5° (black solid line in Figure 9(a)) where it is around 11° for the uncontrolled TORB command (not shown here). It is clear from the figure that the swinging motion was suppressed at

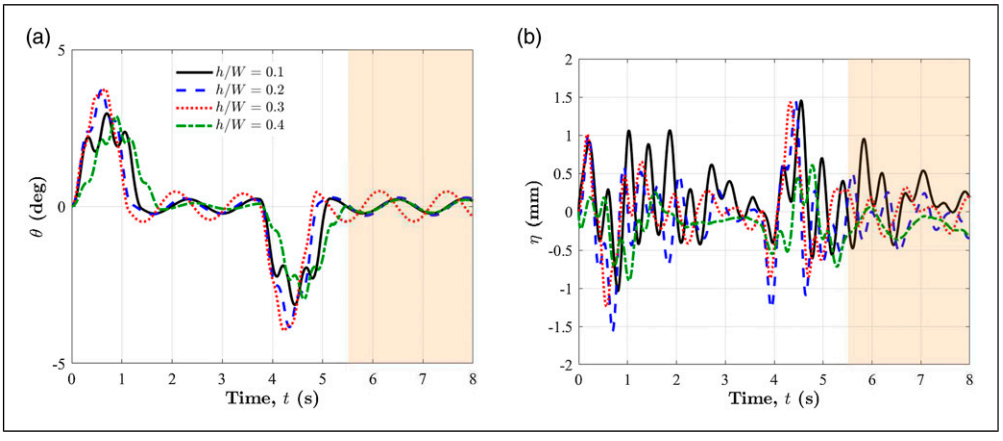

Figure 7. Dynamic responses using the fastest multi-steps input command and different depth ratios, h/W (l/H = 3). (a) Swing angle. (b) Free-surface water level.

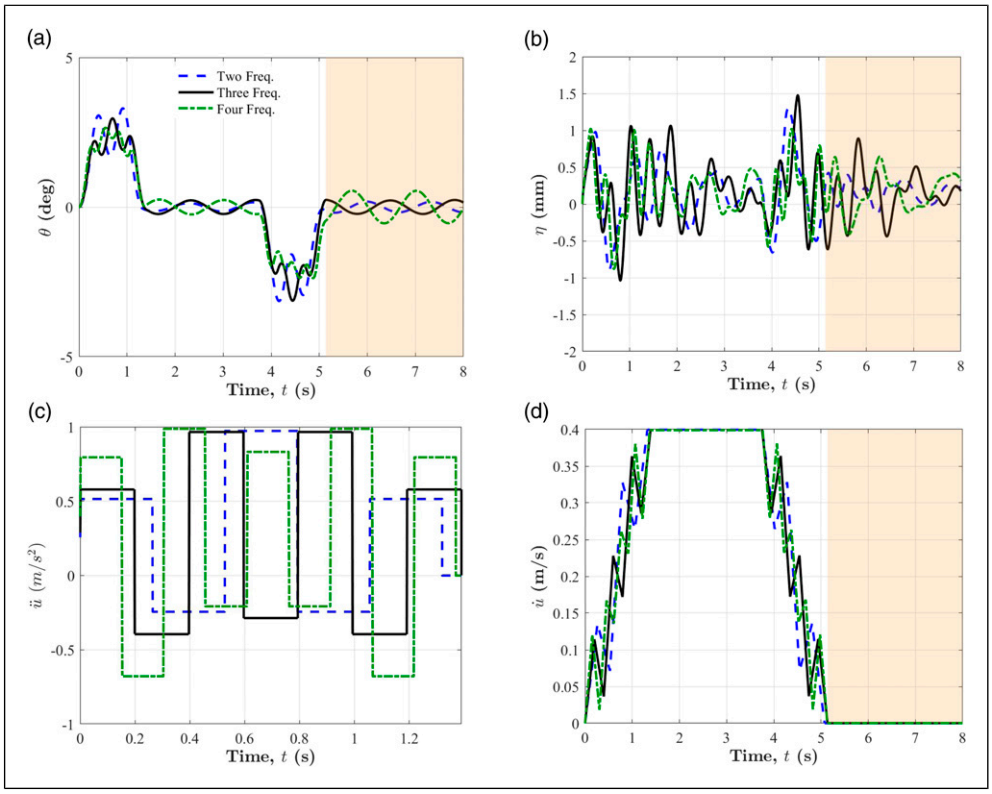

Figure 8. Multi-steps input command profiles designed based on different number of resonant frequencies and their corresponding dynamics responses (h/W = 0.1 and l/H = 3). (a) Swing angle. (b) Free-surface water level. (c) Jib acceleration. (d) Jib velocity.

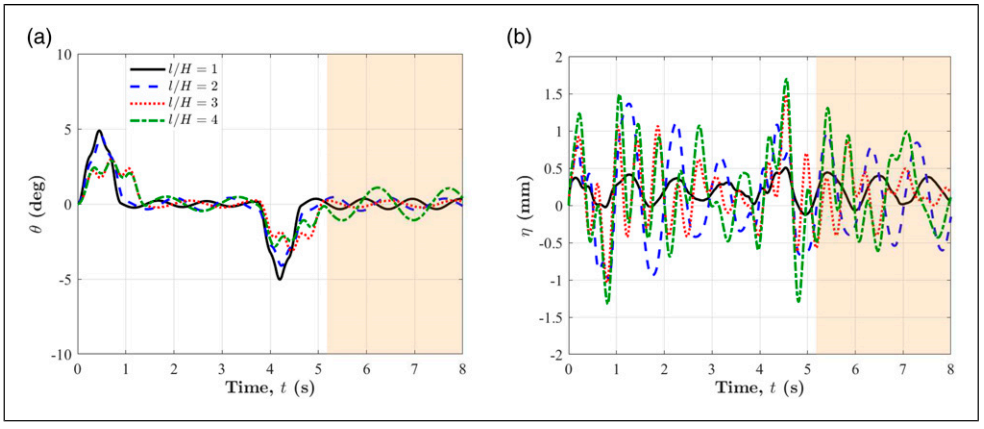

Figure 9. Dynamic responses using the fastest multistep input command and different cable length ratios, l/H (h/W = 0.1). (a) Swing angle. (b) Free-surface water level.

the end of the command stages. The same behavior can be observed for the different cable length ratios, l/H. The increase in the cable length renders a slower response (increases the maneuver time) and reduces the reduction in the water sloshing, Table 3. All the MSICs were designed using three resonant frequencies. All the shaped MSICs use the full system's capabilities and the ones with the fastest response, that is, the smallest maneuver time, are plotted in Figure 9.

4.3. Comparisons with other input shaping techniques

The effectiveness of the proposed MSIC is demonstrated through a comparison with a multimode zero-vibration shaper (MMZV) and a TOZV with respect to maneuver time, transient and residual sloshing reduction, excitation of unmodeled higher sloshing modes, and ease of implementation. A single-mode zero-vibration shaper is

Table 3. Command lengths, maneuver times, and rms values of the free-surface water oscillations for different cable length ratios (T_{TORBs} = 4.15 s).

		Maneuver time		Water level	
l/*H*	τ_a (s)	*T* (s)	Increase (%)	η_{rms} (mm)	Reduction (%)
1	0.89	4.64	11.8	0.2500	91.7
2	0.97	4.72	13.7	0.5929	89.4
3	1.39	5.14	23.9	0.4434	89.6
4	1.43	5.18	24.8	0.6235	88.4

constructed by convolving a sequence of impulses with system input to generate an output with zero-residual vibration (Singer and Seering, 1990; Singhose and Pao, 1997). For a multimode system, convolving sequences of impulses designed for each of the vibrational modes independently generate a sequence of MMZV with 2^N impulses that move the system without residual vibration. This convolved MMZV sequence consists of packed impulses that are difficult to implement in real time and consequently increase the time required to modify the input (by the sum of the damped periods of the canceled modes) and reduce the servo rate performance (Hyde, 1990). Alternatively, one can generate a sequence of $N + 1$ impulses with a command length shorter than the convolved shapers by solving the following set of $2N + 1$ simultaneous nonlinear constraint equations

$$\sum_{k=1}^{m} A_k e^{\zeta_j \omega_j t_k} \sin\left(\omega_j \sqrt{1-\zeta_j^2}\, t_k\right) = 0, \quad \text{for} \quad j = 1, 2, \ldots, N \tag{9a}$$

$$\sum_{k=1}^{m} A_k e^{\zeta_j \omega_j t_k} \cos\left(\omega_j \sqrt{1-\zeta_j^2}\, t_k\right) = 0, \quad \text{for} \quad j = 1, 2, \ldots, N \tag{9b}$$

$$\sum_{k=1}^{m} A_k = a_{\max} \tag{9c}$$

where A_k is the impulse magnitude, t_k is the time at which the impulse occurs, ω_j and ζ_j are the corresponding natural frequency and the damping ratio of the mode j, $m = N + 1$ is the number of required impulses, and N is the number of canceled modes in the vibrational system. The two first equations guarantee the elimination of the residual vibrations where the last equation ensures that none of the generated impulses exceeds the input limitation, for example, maximum acceleration. There are $2(N + 1)$ unknowns of A_k and t_k in $2N + 1$ equations. Therefore, to avoid infinite set of solutions, it is common to set $t_1 = 0$ as the origin specification of the impulses sequence. The nonlinear equations were solved as an optimization problem where the cost function to be minimized is the maneuver time and the nonlinear equality constraints are the nonlinear equations in (9).

The TOZV is an input shaping command that uses the full acceleration capability of the actuator with rapid switching of the command between its maximum and minimum acceleration values (Singhose and Pao, 1997). Using the form of equation (2), the command profile of the TOZV can be written as

$$\ddot{u}(t) = a_{\max} H_{\tau_1} + 2a_{\max} \sum_{k=2}^{m} (-1)^{k-1} H_{\tau_k} \tag{10}$$

where in this case, the time locations τ_k are unknown and can be determined by setting the generalized coordinates and their time derivatives to zero, equations (3) and (4), and ensuring the jib velocity and the traveled distance are not exceeding the predefined values v_f and d, respectively. Because of the transcendental nature of these constraints, the equations may have none, one, or many solutions that satisfying these constraint equations. Therefore, numerical optimization was also used to solve these set of $N + 1$ simultaneous nonlinear equations for the optimal command profile of TOZV.

For the current comparison analysis, the cruising velocity and the total traveled distance were changed to v_f = 1.4 m/s and d = 4 m. Figure 10 shows the responses of the suspended system with $h/W = 0.1$ and $l/H = 3$ when using the MSIC, MMZV, and TOZV. The rms values of the induced wave oscillation, η_{rms}, from TORB, MSIC, MMZV, and TOZV are 2.3709, 0.3215, 0.2426, and 0.5234 mm, respectively. Therefore, the controlled MSIC, MMZV, and TOZV commands result a reduction of 86.4%, 89.8%, and 77.9% in the wave oscillation compared to the TORB command. It is clear from Figure 10(c) and (d) that the MMZV does not use the full actuator capability. For this reason, the transient vibration amplitudes of MMZV are less than the induced amplitudes from MSIC and TOZV. Although the TOZV has a relatively small maneuver time (T = 4.90 s) compared to the MSIC (T = 5.22 s) and MMZV (T = 5.65 s), the TOZV does not guarantee the elimination of the residual vibrations of the higher modes, Figure 10(a) and (b).

Furthermore, the optimal time locations τ_i of the MMZM and TOZV may not be within the sampling time of the actuator hardware. The transient oscillations induced by the sloshing are greater for the TOZV. It is worth noting that it was easy to implement and designed the shaped MSIC which is based on a system of simultaneous linear equation (6), than designing MMZV or TOZV that necessitates the need of using numerical optimization. Given the numerous advantages provided by the proposed MSIC in suppressing the residual sloshing, it provides an attractive alternative to the MMZV and TOZV commands.

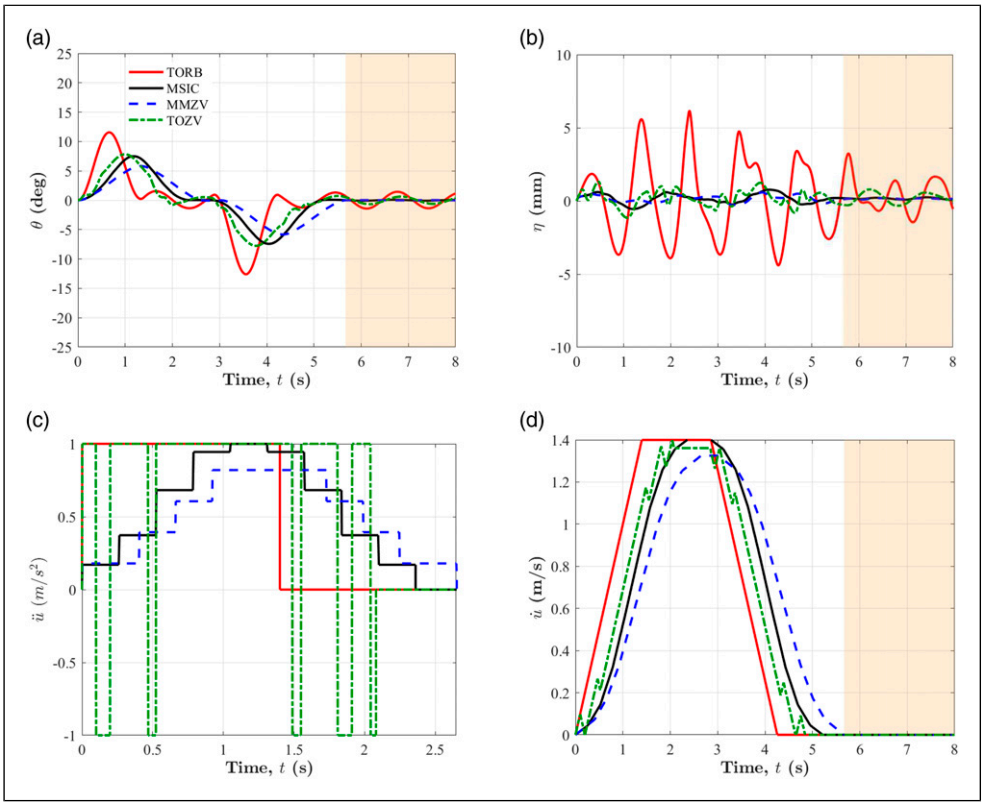

Figure 10. Comparison of the dynamic responses from MSIC, MMZV, and TOZV using four resonant frequencies ($h/W = 0.1$ and $l/H = 3$). (a) Swing angle. (b) Free-surface wave motion. (c) Jib acceleration. (d) Jib velocity. Notes: MSIC: Multi-steps input command; MMZV: multimode zero-vibration; TOZV: time-optimal flexible-body control.

4.4. Sensitivity analysis

The designing of the proposed MSIC depends on the natural frequencies of the system. The uncertainties in measuring the cable length or water depth, the applied assumptions when deriving the mathematical model, and/or the changing of the water depth during the motion will result of modeled frequencies that are not exactly representing the actual values. These variations will result of increase in the residual vibrations. Therefore, parametric sensitivity analyses are conducted to assess these changes in the performance of the shaped command and test its robustness. To perform such analyses, the designed MSIC based on a certain value of the system parameters (cable length and water depth) has to be applied to models while changing one or more of the system parameters.

The robustness or the insensitivity is a measure of the shaped command ability to reduce residual vibrations in the presence of modeling errors. The sensitivity problem of the MSIC can be tackled by several ways (including but not limited to): (i) increasing the command duration of the shaped input command, (ii) adding two fictitious frequencies adjacent to the operating frequency range (analogous to extra-insensitive technique), (iii) adding extra constraints when designing the shaped command such as setting the derivative of the residual vibration amplitude with respect to model parameter, that is, natural frequency, to zero (analogous to zero-vibration derivative technique), and/or (iv) using a larger number of steps, more than the minimum number of required steps $m = 2N + 1$ that needed to satisfy the rest-to-rest maneuvers, where the excess can be used to enhance the robustness. The first three approaches will be considered in the following subsections.

4.4.1. Adjusting command lengths. The dynamics response of a MSIC designed based on a water depth ratio of $h/W = 0.1$ ($\omega_1 = 4.707$ rad/s, $\omega_2 = 6.275$ rad/s, and $\omega_3 = 10.98$ rad/s), a cable length ratio of $l/H = 3$, and different command lengths, $\tau_a = 1.39$ s ($T = 5.14$ s) and $\tau_a = 1.60$ s ($T = 5.35$ s) while changing the water depth or cable length are illustrated in Figure 11. The changing of the water depth certainly changes the sloshing frequencies but has no significant effect on the swinging frequency. Therefore, the command performance in eliminating the swing motion was not degraded when changing the water depth as shown in Figure 11(a) and (b). However, large transient and residual water oscillations were consequently induced. The changing of the cable length has no significant impact on the sloshing frequencies, but it changes dramatically the swing

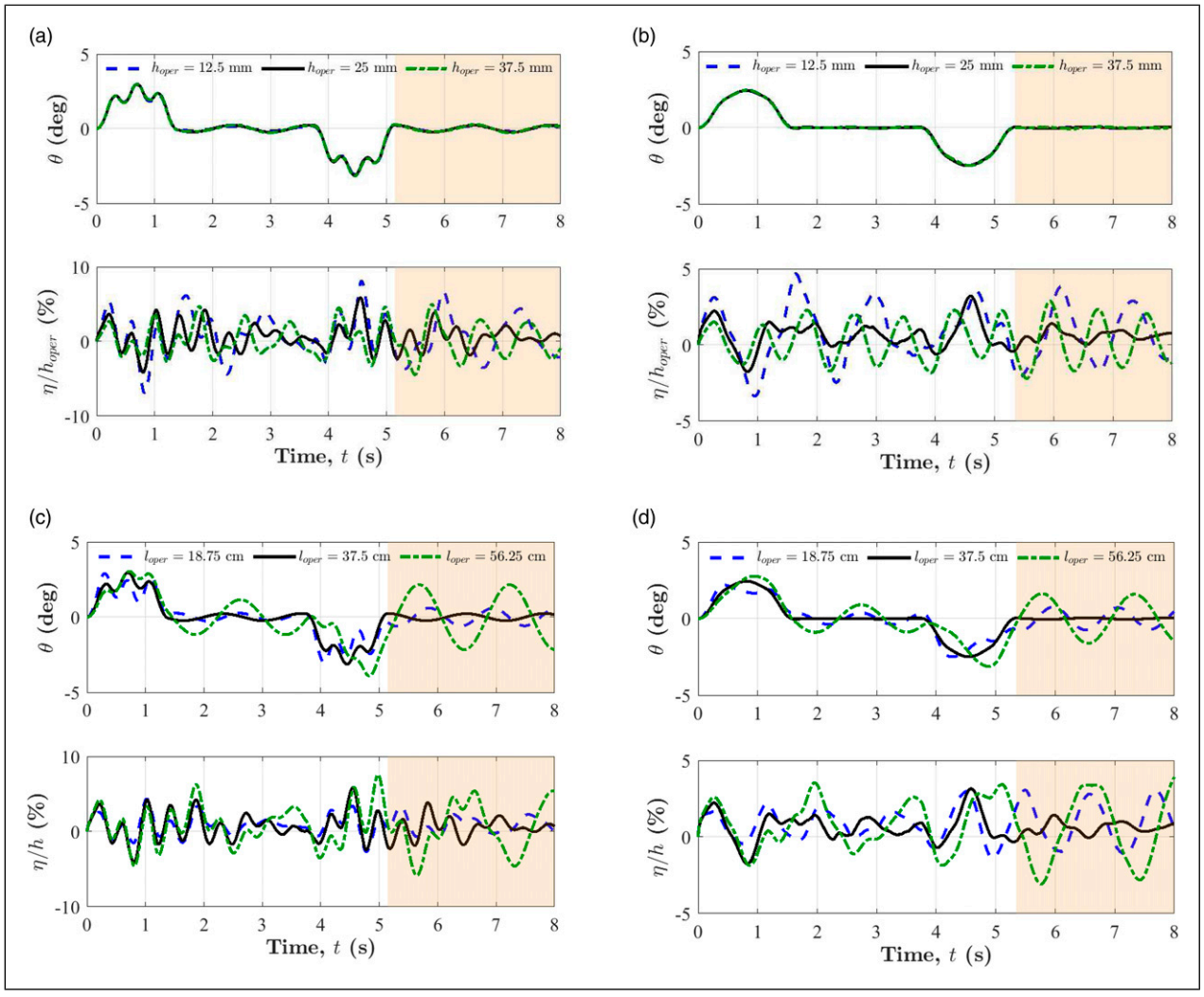

Figure 11. Dynamic response of multi-steps input command when the operating water depth and cable length are ±50% from the designed nominal values for different command lengths (h/W = 0.1 and l/H = 3). (a) h_{nom} = 25 mm, l = 37.5 cm, and τ_a = 1.39 s. (b) h_{nom} = 25 mm, l = 37.5 cm, and τ_a = 1.60 s. (c) h = 25 mm, l_{nom} = 37.5 cm, and τ_a = 1.39 s. (d) h = 25 mm, l_{nom} = 37.5 cm, and τ_a = 1.60 s.

frequency and consequently produces large transient and residual swing oscillation as shown in Figure 11(c) and (d).

4.4.2. MSIC with extra-insensitive. Another approach in making the command more robust is to add two virtual frequencies adjacent to the operating frequency corresponding to different water depths and/or cable lengths. Figure 12 shows the dynamics responses of MSIC with extra-insensitive (MSIC-EI) designed based on a water depth of 25 mm (h/W = 0.1) and a cable length of 37.5 cm with two different command lengths, τ_a = 2.12 s (T = 5.88 s) and τ_a = 2.48 s (T = 6.23 s). The command was designed based on the four resonant frequencies shown in Figure 4(a) in addition to the frequencies 7.844 and 9.413 rad/s corresponding to the depths 12.5 mm and 37.5 mm (13 steps). The performance of MSIC-EI is quite comparable to the performance of MSIC with Zero-Vibration (MSIC-ZV) with a command length of 2.48 s, Figure 14.

4.4.3. MSIC with zero-vibration derivative. The MSIC robustness under variations of the system natural frequencies can be enhanced by adding additional constraints based on setting the derivatives of the residual amplitude with respect to the each of the system frequencies, ω_i, to zero. The vibration amplitude at the end of the command duration is defined as follows

$$\text{Amp} = \sum_{i=1}^{N} \sqrt{q_i^2(\tau_a) + \left(\frac{\dot{q}_i(\tau_a)}{\omega_i}\right)^2} \qquad (11)$$

The condition of $d(\text{Amp})/d\omega_i = 0$ is satisfied if

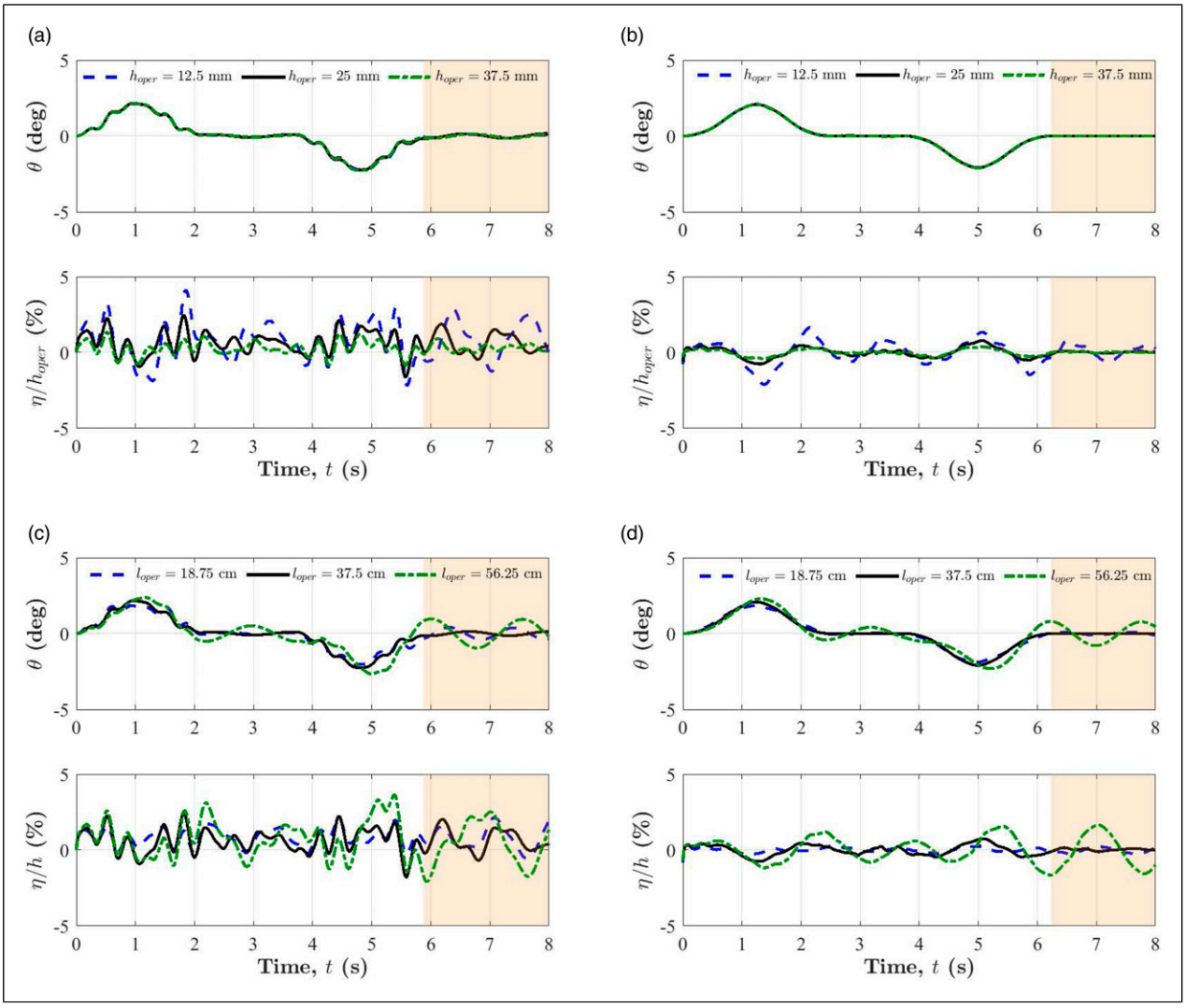

Figure 12. Dynamic responses of multi-steps input command with extra-insensitive when the operating water depth and cable length are ±50% from the designed nominal values for different command lengths (h/W = 0.1 and l/H = 3). (a) h_{nom} = 25 mm, l = 37.5 cm, and τ_a = 2.12 s. (b) h_{nom} = 25 mm, l = 37.5 cm, and τ_a = 2.48 s. (c) h = 25 mm, l_{nom} = 37.5 cm, and τ_a = 2.12 s. (d) h = 25 mm, l_{nom} = 37.5 cm, and τ_a = 2.48 s.

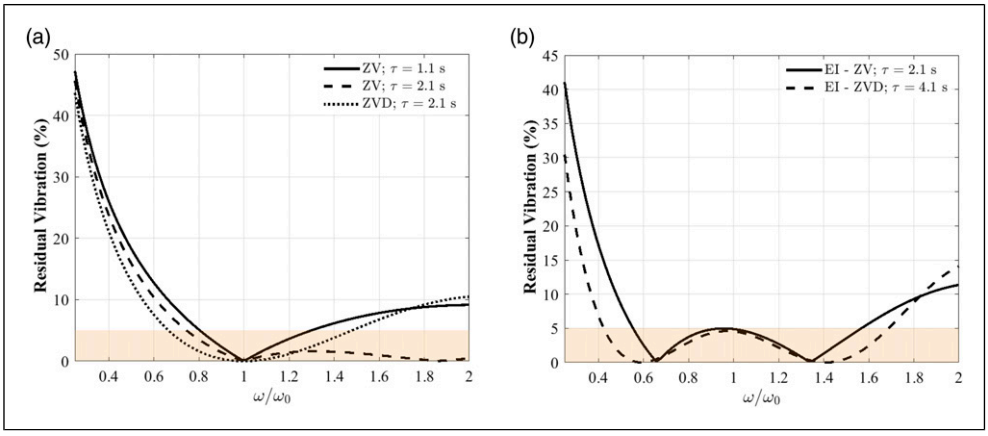

Figure 13. Sensitivity curve of the residual vibration amplitude versus the variation of the operating frequency with respect to the modeling frequency using MSIC- (a) ZVD and (b) EI. Note: MSIC-ZVD: MSIC with zero-vibration derivative; MSIC-EI: multi-steps input command with extra-insensitive.

$$\frac{dq_i(\tau_a)}{d\omega_i} = \frac{p_i}{\omega_i}\sum_{k=1}^{m}(A_k - A_{k-1})\sin(\omega_i(\tau_a - \tau_k))(\tau_a - \tau_k)H_{\tau_k} = 0 \quad (12a)$$

$$\frac{d(\dot{q}_i(\tau_a)/\omega_i)}{d\omega_i} = \frac{p_i}{\omega_i}\sum_{k=1}^{m}(A_k - A_{k-1})\cos(\omega_i(\tau_a - \tau_k))(\tau_a - \tau_k)H_{\tau_k} = 0 \quad (12b)$$

Therefore, $m = 4N + 1$ steps are needed in equation (2) to satisfy the rest-to-rest constraints, that is, $q_i(\tau_a) = 0$ and $\dot{q}_i(\tau_a) = 0$, the insensitivity conditions, equation (12), and the end velocity constraint, equation (5). Imposing these conditions results a linear system of simultaneous equations $\mathbf{Mc} = \mathbf{b}$ where $\mathbf{c} = \{A_1 \quad A_2 - A_1 \quad \cdots \quad A_{4N+1} - A_{4N}\}^T$ and $\mathbf{b} = \{0 \quad \cdots \quad 0 \quad v_f/\Delta\tau\}^T$ are column vectors and matrix $\mathbf{M}$ is defined as

$$\begin{aligned}
\mathbf{M}(4i-3,k) &= 1 - \cos(\omega_i(\tau_a - (k-1)\Delta\tau)) \\
\mathbf{M}(4i-2,k) &= \sin(\omega_i(\tau_a - (k-1)\Delta\tau)) \\
\mathbf{M}(4i-1,k) &= \sin(\omega_i(\tau_a - (k-1)\Delta\tau))(\tau_a - (k-1)\Delta\tau) \\
\mathbf{M}(4i,k)) &= \cos(\omega_i(\tau_a - (k-1)\Delta\tau))(\tau_a - (k-1)\Delta\tau) \\
\mathbf{M}(4N+1,k) &= 4N + 2 - k
\end{aligned} \quad (13)$$

where $i = 1, 2, \ldots, N$ and $k = 1, 2, \ldots, 4N + 1$. The concepts of using input command to produce zero-residual vibration and then adding additional constraints are similar, respectively, to the concepts of zero vibration (ZV) and zero-vibration

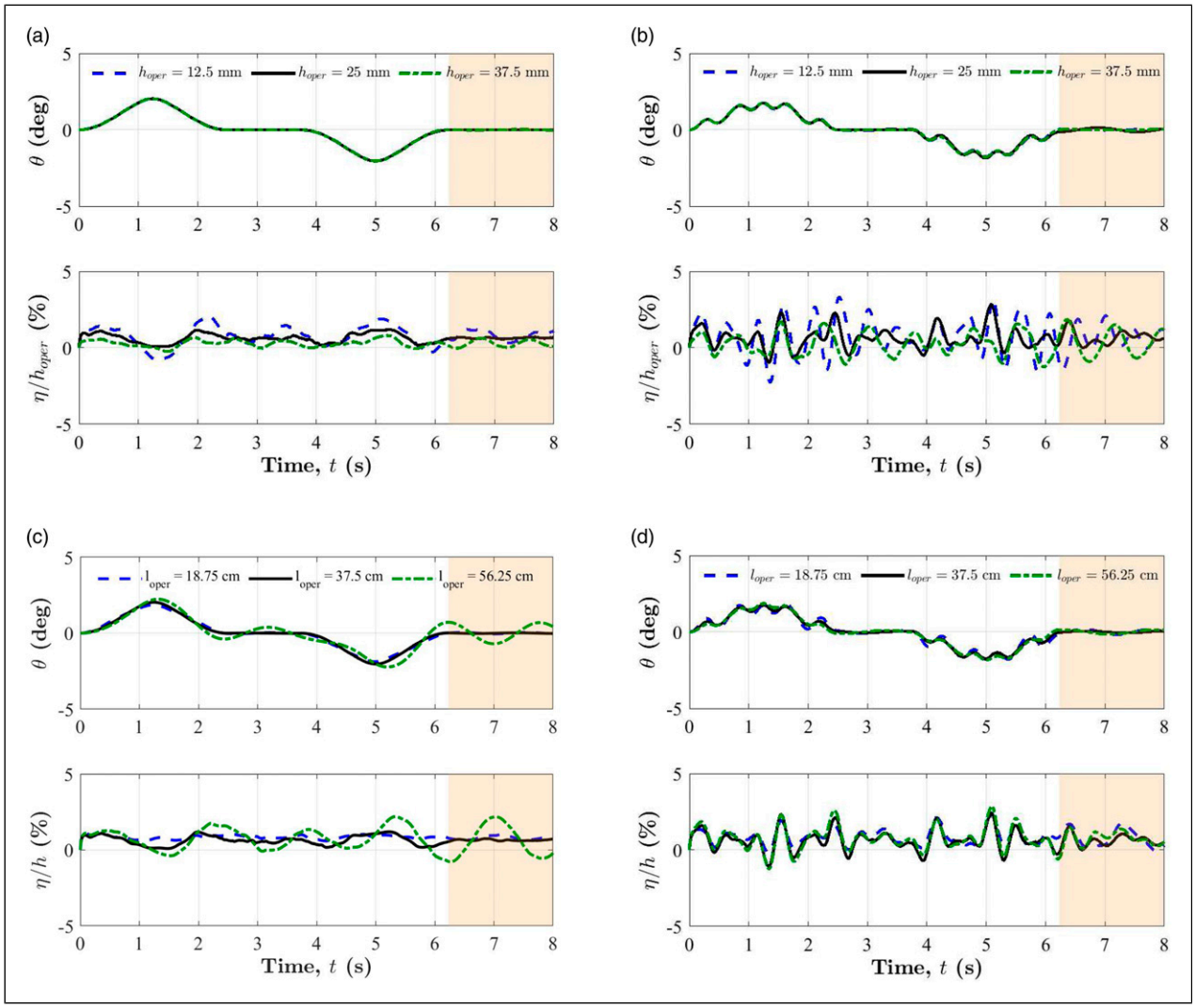

Figure 14. Dynamics responses of MSIC-ZV and MSIC-ZVD when the operating water depth and cable length are ±50% from the designed nominal values ($h/W = 0.1$, $l/H = 3$ and $\tau_a = 2.48$ s). (a) MSIC-ZV: $h_{nom} = 25$ mm and $l = 37.5$ cm. (b) MSIC-ZVD: $h_{nom} = 25$ mm and $l = 37.5$ cm. (c) MSIC-ZV: $h = 25$ mm and $l_{nom} = 37.5$ cm. (d) MSIC-ZVD: $h = 25$ mm and $l_{nom} = 37.5$ cm. Notes: MSIC-ZV: MSIC with Zero-Vibration; MSIC-ZVD: MSIC with Zero-Vibration-Derivative.

derivative (ZVD) input shapers proposed by Singer and Seering (1990).

The performance of the MSIC when adding the zero-derivative constraints (denoted as MSIC-ZVD) compared with MSIC satisfying only the zero-vibration residual (denoted as MSIC-ZV) is shown in Figure 13(a). A fully settled system is achieved if the oscillation is less than a five percent level (the shaded area in Figure 13). These commands are designed based on the same input system capability and a modeling frequency of $\omega_0 = \pi$ rad/s. The command length of the robust command ZVD is double of the ZV command. The MSIC-ZV is robust for system frequency variations from -20% to $+30\%$ where the MSIC-ZVD is robust for variations from -30% to $+50\%$ of the system frequency, Figure 13(a). To demonstrate the effectiveness of the MSIC-ZVD when the MSIC-ZV has the same command length, the latter was also shown in Figure 13(a) which has a robustness for a frequency variation from -25% to infinity. Figure 13(b) shows the sensitivity curve of the MSIC-ZV-EI and MSIC-ZVD-EI when two frequencies in the limit of the operating range are considered as modeling frequencies. This increases the robustness to the ranges -40% to $+60\%$ for MSIC-ZV-EI and -60% to $+70\%$ for MSIC-ZVD-EI, Figure 13(b).

Figure 14 shows the dynamics responses of MSIC-ZV and MSIC-ZVD designed based on a water depth of 25 mm ($h/W = 0.1$), a cable length of 37.5 cm, and a command length of $\tau_a = 2.48$ s ($T = 6.23$ s). The MSIC-ZV was designed based on the four resonant frequencies (9 steps) shown in Figure 4(a) where the MSIC-ZVD was also designed based on the same four resonant frequencies in addition to using the conditions of equation (12) for ω_1 and ω_2 (results of 13 steps command) corresponding to the swinging and the fundamental sloshing frequencies, respectively. Changing of the water depth does not affect the swing response. MSIC-ZV performance based on the swing

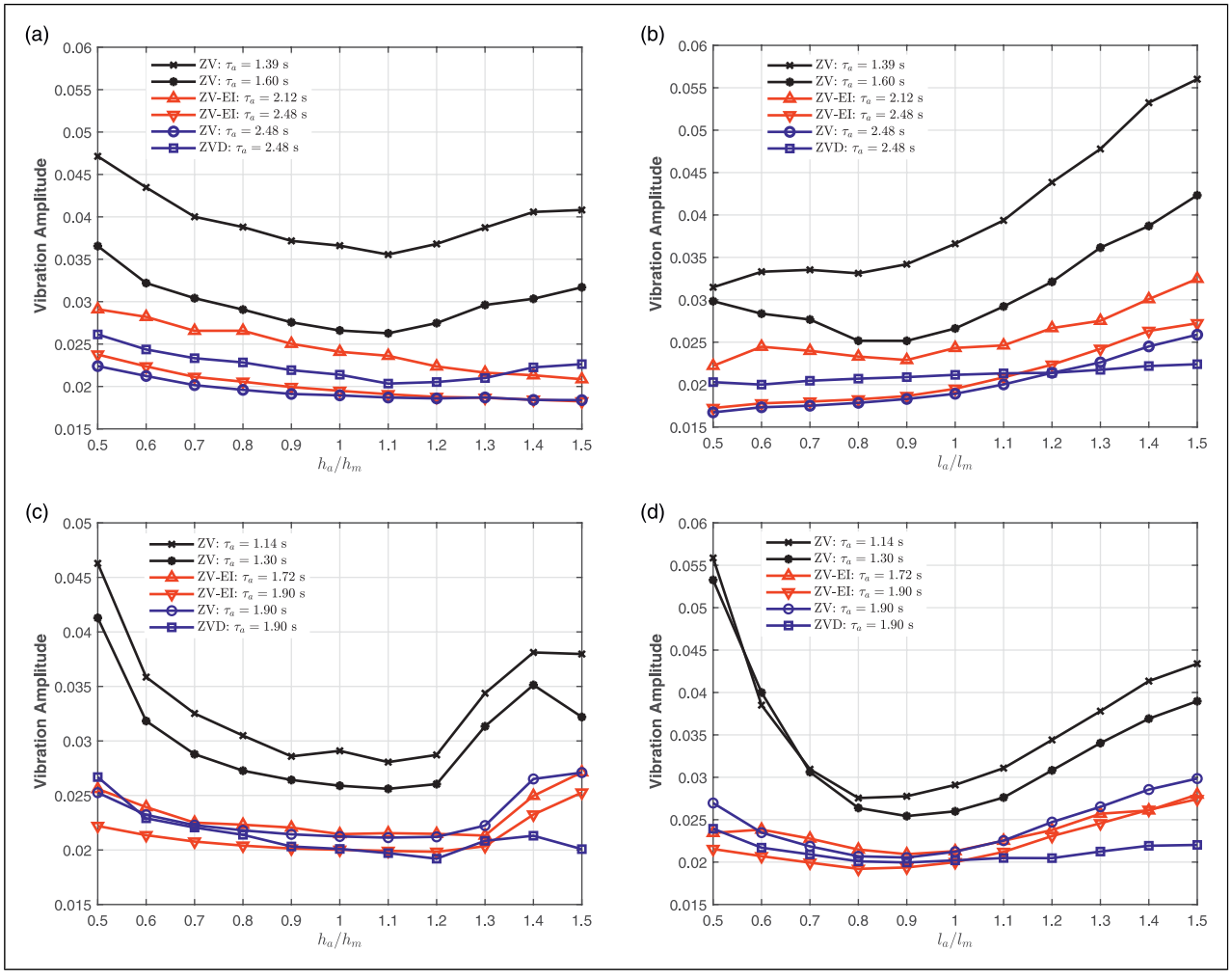

Figure 15. Sensitivity analysis for different robust multi-steps input commands with respect to the changes in the operating water depth and cable length. (a) $h_m = 25$ mm and $l = 37.5$ cm. (b) $h = 25$ mm and $l_m = 37.5$ cm. (c) $h_m = 75$ mm and $l = 37.5$ cm. (c) $h = 75$ mm and $l_m = 37.5$ cm.

motion and water oscillation with the changing of the water depth is superior than the performance of the MSIC-ZVD as shown in Figure 14(a) compared to Figure 14(b). In contrast, MSIC-ZVD shows a superior robust performance with the changes in the cable length than the MSIC-ZV, Figure 14(d) compared to Figure 14(c).

4.4.4. General remarks. Because the objective is to suppress the induced transient and residual water sloshing, the vibration amplitude is quantified as follows

$$\text{Vib.Amp.} = \theta_{\text{rms}} + \frac{\eta_{\text{rms}}}{h_a} \tag{14}$$

where θ_{rms} (in radian) and η_{rms} are the rms of the sloshing oscillation of the swing angle and water level of the free surface, respectively, and h_a is the actual depth. The sensitivity curve for the different robust MSICs is illustrated in Figure 15. As overall observation, the residual vibrations are reduced and the command robustness is enhanced with the increasing in the command length. The performance of the MSIC degrades as the variations of the frequencies from the modeled frequency become greater.

Figure 15(a) and (b) shows the sensitivity of the MSICs with water depth and cable length uncertainties in a shallow water-filled container, $h/W = 0.1$, respectively. Command performance is degraded when the operating depth is lower than the modeling depth. Therefore, it is recommended to underestimate the water depth when designing the MSIC. Large residual and transient vibrations were produced when the operating cable length was greater than the nominal length for MSIC-ZV with small command length. Hence, it is recommended to overestimate the cable length for a fast MSIC in a shallow container. However, the changes in the cable length do not influence the commands performance of MSIC-EI, MSIC-ZVD, and MSIC-ZV with a larger command length.

The sensitivity of the shaped commands with the water depth and cable length uncertainties in a deep water-filled container, $h/W = 0.3$, is shown in Figure 15(c) and (d), respectively. The vibration amplitudes were reduced compared to a shallow water-filled container, $h/W = 0.1$. Same conclusions drawn from the shallow water-filled container are observed in the figures for the case of deep water-filled container. However, the command sensitivity with the changes in the cable length suggests underestimating the length of the cable when designing a fast MSIC-ZV.

Conclusions

A shaped command based on equidistant multi-steps segments for zero-residual vibrations at the end of a command duration in all modes of a multimode system was proposed. The transient water oscillation and residual sloshing of suspended moving water-filled container were suppressed using the proposed shaped command to test its performance and effectiveness. The dynamic of the induced sloshing was modeled by means of FEM using fluid–structure interaction and multi-body dynamics. The uncertainties of the frequency variation because of changing in the water depth and cable length were investigated. The time penalty of introducing the shaped command is negligible compared to the reduction in the transient and residual water sloshing. Unlike previous works which only consider the fundamental sloshing frequency, considering the higher sloshing frequencies in command-designing provides additional elimination of the residual water sloshing. The command duration of the MSIC depends only on the natural frequencies unlike the classical input shapers. This ability of adjusting the command duration makes the MSIC attractive in selecting an optimal command that compensates between the transient sloshing reduction, total maneuver time, and command robustness.

A sensitivity analysis, which demonstrates how much residual vibrations induced when error in estimating the system frequency is present, was also demonstrated. For small changes or uncertainties in the water depth and cable length, a considerable amount of residual vibration was induced. The MSIC robustness was enhanced by increasing the command length, adding zero-derivative constraints at the modeled frequencies, and/or considering the frequencies limits as modeling frequencies in command-designing to widen the operational range. Therefore, the variations of the operating frequencies from the modeling frequency because of the embedded nonlinearities in the system, the variation of the system parameters (such the case of the changes in the water depth of a conveying water-filled container), model assumptions, etc. do not incur significant residual vibrations at the end of the maneuver.

No general statement can be made regarding the application of the MSIC to nonlinear systems because each nonlinearity poses unique problems. However, the linear resonant frequencies can be used to design the shaped command as long as the system is varying slowly such that the linearity assumption is applied. The variation of the natural frequency because of the nonlinearity does not interfere with the vibration reduction effects because of the robustness to the frequencies uncertainty. The reduction of the vibration amplitude of the suspended water-filled container, giving that the simulation model is highly nonlinear, demonstrates the effectiveness of the MSIC in the presence of certain system nonlinearities.

Declaration of conflicting interests

The author(s) declared no potential conflicts of interest with respect to the research, authorship, and/or publication of this article.

Funding

The author(s) received no financial support for the research, authorship, and/or publication of this article.

ORCID iD

Abdullah Alshaya https://orcid.org/0000-0002-9105-5300

References

Aboel-Hassan A, Arafa M and Nassef A (2009) Design and optimization of input shapers for liquid slosh suppression. *Journal of Sound and Vibration* 320(1): 1–15.

Alhazza KA and Masoud ZN (2016) Waveform command shaping control of multimode systems. *Journal of Sound and Vibration* 363: 126–140.

AlSaibie A and Singhose (2013) Experimental testing of liquid slosh suppression in a suspended container with compound-pendulum dynamics. In: 9th Asian control conference (ASCC), Istanbul, Turkey, 23–26 June 2013. IEEE.

Alshaya A and Alghanim K (2020) Command shaping for sloshing suppression of a suspended liquid container. *Journal of Dynamic Systems, Measurement, and Control* 142: 121003.

Alshaya A and Almujarrab D (2020) A smooth polynomial shaped command for sloshing suppression of a suspended liquid container. *Transactions of the Institute of Measurement and Control* 43: 0142331220949304.

Arafa M (2007) Finite element analysis of sloshing in rectangular liquid-filled tanks. *Journal of Vibration and Control* 13: 883–903.

Baozeng Y and Lemei Z (2014) Hybrid control of liquid-filled spacecraft maneuvers by dynamic inversion and input shaping. *AIAA Journal* 52(3): 618–626.

Biagiotti L, Chiaravalli D, Moriello L, et al. (2018) A plug-in feedforward control for sloshing suppression in robotic teleoperation tasks. *2018 IEEE/RSJ International Conference on Intelligent Robots and Systems (IROS)*: 5855–5860. DOI: 10.1109/IROS.2018.8593962.

Brar GS and Singh S (2014) An experimental and cfd analysis of sloshing in a tanker. *Procedia Technology* 14: 490–496.

COMSOL (2019) *Comsol Multiphysics Reference Manual, comsol, inc*. www.comsol.com.

Cho JR and Lee HW (2004) Numerical study on liquid sloshing in baffled tank by nonlinear finite element method. *Computer Methods in Applied Mechanics and Engineering* 193: 2581–2598.

Graham EW and Rodriguez AM (1952) The characteristics of fuel motion which affect airplane dynamics. *Journal of Applied Mechanics* 19: 381–388.

Hasheminejad SM, Mohammadi M and Jarrahi M (2010) Fluid—structure interaction in partially filled liquid containers: a comparative review of numerical approaches. *Journal of Fluids and Structures* 39: 739–746.

Hasheminejad SM, Mohammadi MM and Jarrahi M (2014) Liquid sloshing in partly-filled laterally-excited circular tanks equipped with baffles. *Journal of Fluids and Structures* 44: 97–114.

Huang J and Zhao X (2018) Control of three-dimensional nonlinear slosh in moving rectangular containers. *Journal of Dynamic Systems, Measurement, and Control* 140: 081016.

Hyde JMS (1990) Using input command pre-shaping to suppress multiple mode vibration. In: Proceedings 1991 IEEE international conference on robotics and automation, Sacramento, CA, 9–11 April 1991. IEEE.

Ibrahim RA (2005) *Liquid Sloshing Dynamics: Theory and Applications*. 1st edition. New York: Cambridge University Press.

Kaneshige A, Miyoshi T and Terashima K (2009) The development of an autonomous mobile overhead crane system for the liquid tank transfer. In: IEEE/ASME international conference on advanced intelligent mechatronics, Singapore, 14–17 July 2009, pp. 630–635. IEEE.

Masoud ZN and Alhazza KA (2017) A smooth multimode waveform command shaping control with selectable command length. *Journal of Sound and Vibration* 397: 1–16.

Mohamed Z and Tokhi M (2003) Command shaping techniques for vibration control of a flexible robot manipulator. *Mechatronics* 39: 1039–1047.

Murthy AS, Kivila A and Singhose W (2012) Slosh suppression of a liquid in a suspended container using robust input shaping. In: 19th international congress on sound and vibration. Vilnius, Lithuania, 1–8 January 2012. Vilnius, Lithuania: International Institute of Acoustics and Vibration (IIAV).

Singer NC and Seering WP (1992) An extension of command shaping methods for controlling residual vibration using frequency sampling. *Proceedings 1992 IEEE International Conference on Robotics and Automation* 1: 800–805.

Pridgen B, Bai K and Singhose W (2013) Shaping container motion for multimode and robust slosh suppression. *Journal of Spacecraft and Rockets* 50(2): 440–448.

Reyhanoglu M and Rubio Hervas J (2013) Nonlinear modeling and control of slosh in liquid container transfer via a PPR robot. *Communications in Nonlinear Science and Numerical Simulation* 18(6): 1481–1490.

Singer NC and Seering WP (1990) Preshaping command inputs to reduce system vibration. *Journal of Dynamic Systems, Measurement, and Control* 112(1): 76–82.

Singh T and Vadali SR (1995) Robust time-delay control of multimode systems. *International Journal of Control* 62(6): 1319–1339.

Singhose W and Pao L (1997) A comparison of input shaping and time-optimal flexible-body control. *Control Engineering Practice* 5(4): 459–467.

Vaughan J, Yano A and Singhose W (2008) Comparison of robust input shapers. *Journal of Sound and Vibration* 315(4): 797–815.

Wang W, Peng Y, Zhou Y, et al. (2016) Liquid sloshing in partly-filled laterally-excited cylindrical tanks equipped with multi baffles. *Applied Ocean Research* 59: 543–563.

Xing B and Huang J (2020) Control of pendulum-sloshing dynamics in suspended liquid containers. *IEEE Transactions on Industrial Electronics* 68: 5146–5154.

Yano K and Terashima K (2001) Robust liquid container transfer control for complete sloshing suppression. *IEEE Transactions on Control Systems Technology* 9(3): 483–493.

Zang Q and Huang J (2015) Dynamics and control of three-dimensional slosh in a moving rectangular liquid container undergoing planar excitations. *IEEE Transactions on Industrial Electronics* 62(4): 2309–2318.

Zang Q, Huang J and Liang Z (2015) Slosh suppression for infinite modes in a moving liquid container. *IEEE/ASME Transactions on Mechatronics* 20(1): 217–225.

Notations

A_k Magnitudes of the multi-steps input command, $\ddot{u}(t)$
$a_{\max}$ Jib maximum acceleration
d Travel distance
H Container height
H_{τ_k} Heaviside function, $H_{\tau_k} = H(t - \tau_k)$
h Water filling level
l Length of the rigid link
m Number of equidistant segments in MSIC
$q_i(t)$ Principal (decoupled) modal coordinates
s_a, s_c, s_d Travel distance of the acceleration, cruising, and deceleration stages
T Total maneuver time
t Time coordinate
$\ddot{u}(t)$ Jib horizontal acceleration
v_f Jib maximum velocity
W Container width
$\theta(t)$ Swinging angle in xy-plane measured clockwise from vertical y-direction
θ_{rms} RMS of the total vibrations of the swing angle
ρ Water density
τ_a, τ_c, τ_d Time interval of the acceleration, cruising, and deceleration stages
$\Delta\tau$ Time segment of the MSIC
$\eta(x, t)$ Free-surface water elevation from its undistributed height
η_{rms} RMS of the total vibrations of the free-surface water level
ω_i Natural frequency of the suspended system
$(\dot{})$ Time derivative, d/dt